

A FULLY AUTOMATED SCHEME FOR BREAST DENSITY ESTIMATION AND ASYMMETRY DETECTION OF MAMMOGRAMS

Stylianos Tzikopoulos, Harris Georgiou, Michael Mavroforakis, Sergios Theodoridis

National and Kapodistrian University of Athens, Dept. of Informatics and Telecommunications,
Panepistimiopolis, Ilissia, Athens 15784, Greece,
{stzikop, xgeorgio, mmavrof, stheodor}@di.uoa.gr

ABSTRACT

This paper presents a fully automated scheme for breast density estimation and asymmetry detection on mammographic images. Image preprocessing and segmentation techniques are first applied to the image, in order to extract the features for the breast density categorization. Also a new fractal-related feature is proposed for the classification. The classification to 3 classes is realized according to classification and regression trees (CARTs). The same segmentation result is used to extract a set of new statistical features for each breast; the difference of these feature values, between the two images of each pair of mammograms, are estimated and the asymmetric pairs are detected according to a modified version of k-nearest neighbor classifier. This composite method has been implemented and applied to miniMIAS database, consisting of 322 mediolateral oblique (MLO) view mammograms, obtained via a digitization procedure. The results are very promising, showing equal or higher success rates compared to other related algorithms in the literature, despite the fact that some of them use only small portions of the specific database. In contrast our methodology is applied to the complete datatabase.

1. INTRODUCTION

Breast cancer, i.e., a malignant tumor developed from breast cells, is considered to be one of the major causes for the increase in mortality among women, especially in developed countries. More specifically, breast cancer is the second most common type of cancer and the fifth most common cause of cancer death [13].

While mammography has been proved to be the most effective and reliable method for early breast cancer detection [15], the large number of mammograms, generated by population screening, must be interpreted and diagnosed by a relatively small number of radiologists. This is also one of the reasons why it is widely accepted today that automated Computer Aided Diagnosis (CAD) systems are starting to play an important role in modern medical practices.

Most of the CAD systems try to detect abnormalities based on a single mammographic image and on an objective abstract model of the abnormalities. However, there is a high correlation between high breast parenchymal density and high risk of breast cancer [20]. Thus, mammographic images with high breast density value should be examined more carefully by the radiologists, creating a need for automatic breast parenchymal density estimation algorithms. In [11], such algorithms in the literature are presented and a new technique, introducing a histogram distance metric, achieves good results. Some existing algorithms, e.g., [2, 14], use

the texture information of mammograms, in order to extract more features for the breast density estimation.

Radiologists also pay attention to possible asymmetries between the left and the right breast in a pair of mammograms, as they can provide clues about the presence of early signs of tumors [8]. In order to help the radiologists, many CAD systems analyze the images of a mammogram pair and detect asymmetric regions by applying some type of alignment and direct comparison [21]. In [6], a new directional analysis method is proposed, using Gabor wavelets, in order to detect possible asymmetries.

In this work, a new breast parenchymal density estimation algorithm is proposed, using segmentation, first order statistics and fractal analysis of the mammographic image for the extraction of new statistical features, while the classification task is performed using Classification and Regression Trees (CARTs). Furthermore, a new algorithm is proposed for breast asymmetry detection, using the feature values already extracted from the breast parenchymal density estimation step, using a modified version of k-nearest neighbor classifier. Both techniques achieve high success rates, often higher than the corresponding values of other algorithms in bibliography, while they use simpler and faster feature extraction methods.

The rest of this paper is organized as follows. In section 2, the mammographic image database used is presented. The breast parenchymal density estimation method and the asymmetry detection algorithm are described in section 3. Section 4 presents the results obtained by the two proposed algorithms and, finally, the discussion and conclusions are presented in section 5.

2. DATASET

The new methodology presented in this work was applied on miniMIAS database [16], available online freely for scientific purposes and consisting of 161 pairs of mediolateral oblique (MLO) view mammograms. The images of the database originated as the product of a film-screen mammogram process in the United Kingdom National Breast Screening Program. The films were digitized and the corresponding images were annotated according to their breast density by expert radiologists, using three distinct classes: Fatty (F) (106 images), Fatty-Glandular (G) (104 images) and Dense-Glandular (D) (112 images), similar to [12]. Any abnormalities were also detected and described, including calcifications, well-defined, spiculated or ill-defined masses, architectural distortions or asymmetries. Each pair of images of the database is annotated as Symmetric (146 pairs) or Asymmetric (15 pairs). The severity of each abnormality is provided, i.e., benignancy or malignancy.

A typical mammographic image is shown in figure 1a. The presence of high noise is readily observed; this makes the segmentation of the image a demanding task. Moreover, speckle noise was added through the original digitization processing of the film mammograms. The original 0.2 mm/pixel images were resized to 0.4 mm/pixel, as in [10] and [11], in order to reduce the required computational time. The initial bit depth of 8 bits was preserved.

3. METHODS

3.1 Breast Density Estimation

3.1.1 Image Preprocessing

The noise of the image, e.g., high intensity scanning labels, or tape artifacts, is detected and excluded from the remaining processing, using the same concept as in [11]. Figure 1b shows an example of this process.

In order to estimate the breast boundary, the algorithm in [11] was implemented. The key idea of the algorithm is that the skin-air boundary is the smoothest section of identical pixels near the breast edge, detected using a thresholding technique. A result of the algorithm is presented in figure 1c.

The pectoral muscle, which is the high-intensity triangular region across the upper posterior (left) margin of the image, appeared only in MLO view of left-breast mammograms, is detected according to [10], with the modifications and improvements of [18]. An example is presented in figure 1d.

Besides the noise segmentation techniques already presented, image processing techniques are also applied for the improvement of the overall image quality. Specifically, a gaussian smoothing filter [7] with variable kernel size $hsize$ and standard deviation $sigma$ is applied on each image, in order to remove the noise. Subsequently, an unsharp filter

[7] with mask $h_{UNSHARP} = \frac{1}{1+a} \begin{bmatrix} -a & a-1 & -a \\ a-1 & a+5 & a-1 \\ -a & a-1 & -a \end{bmatrix}$ of

variable parameter $alpha$ is applied for edge enhancement. The above parameters were automatically tuned according to the following scheme. The following values were given to the variables and, for each combination of values, the success rate of the breast density estimation technique was recorded:

- $hsize$: 3x3, 5x5, 7x7, 9x9, 11x11 (pixels x pixels)
- $sigma$: 0.1, 0.4, 0.7, 1.0
- $alpha$: 0.1, 0.4, 0.7, 1.0

The values that achieved the best success rate were the $hsize$ 7x7, $sigma$ 0.4 and $alpha$ 0.7; these best values were used as the baseline for enhancing all the images in the database prior to any breast segmentation and parenchymal analysis.

3.1.2 Feature Estimation

The previously proposed methodology was applied to each mammogram of the miniMIAS database and the results are illustrated in figure 1, showing:

- The initial I image (figure 1a).
- The background area, labels and artifacts have been excluded, to obtain the $Back$ area (figure 1b).
- The human-tissue HuT area (figure 1c), which has been obtained after extracting background, labels, artifacts and noise from the initial image.

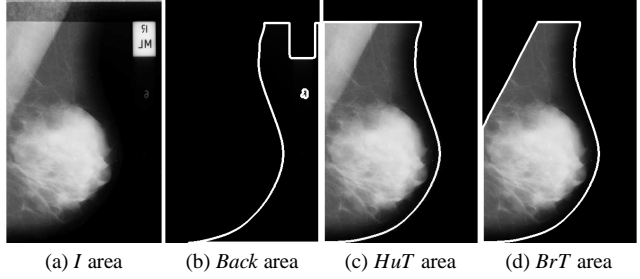


Figure 1: a) Initial Image I , b) background $Back$, c) tissue-rich area HuT and d) breast tissue area BrT

- The segmented breast tissue BrT area (figure 1d), which has been obtained after extracting the pectoral muscle from the human-tissue HuT area.

In order to analyze and model the overall noise levels in the image, the mean and variance of the pixel intensity values are estimated in the $Back$ area (no tissue or artifacts), using equations (1)-(2):

$$F_1 = \mu_{Back} = \frac{\sum_{(i,j) \in Back} I(i,j)}{N(Back)} \quad (1)$$

$$F_2 = \sigma_{Back}^2 = \frac{\sum_{(i,j) \in Back} (I(i,j) - \mu_{Back})^2}{N(Back)} \quad (2)$$

where $N(R)$ is the number of pixels in region R .

Then estimate the synthetic features F_3 and F_4 for the breast tissue (BrT) area, using equations (3)-(4):

$$F_3 = \frac{S_{BrT}}{N(BrT)} \quad (3)$$

$$F_4 = \frac{P_{BrT}}{\mu_{BrT}^2} \quad (4)$$

where S_{BrT} is the surface and P_{BrT} the power of the BrT area and can be found according to equations (5)-(6)

$$S_{BrT} = \sum_{(x,y) \in BrT} I(x,y) + 1 + |I(x+1,y) - I(x,y)| + |I(x,y+1) - I(x,y)| \quad (5)$$

$$P_{BrT} = \sum_{(x,y) \in BrT} |I(x,y)|^2 \quad (6)$$

Next, an algorithm for the computation of the fractal-related feature, based on the power spectrum [7] of the image is provided. The initial image is resized to the lower resolution of 1.6mm/pixel, after placing black (zero-valued) pixels to the non- HuT area. The absolute values of the Fourier transform of the derived image are estimated and averaged over the four quarters. The estimated image is cropped to become square and the logarithmic values over the main diagonal of the image are extracted. An exponential function $f(x) = A \exp(Bx) + C$ is fitted to the extracted data and the feature $F_5 = B$ is obtained, as the feature related to the fractal exponent of the texture of the human tissue [9].

Next, the human tissue HuT is used to perform the minimum cross entropy (MCE) thresholding [4] three times, according to the following scheme:

- T is the (baseline) threshold derived from MCE at gray level range $[1, 2^8 - 1]$

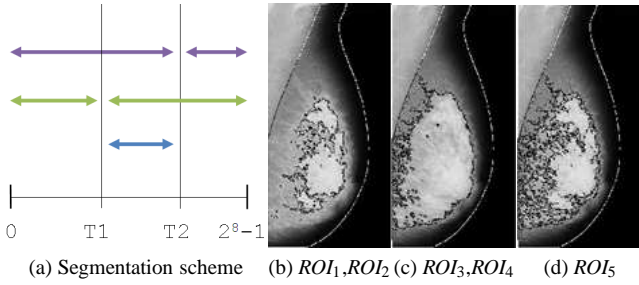


Figure 2: a) Segmentation scheme, b) ROI_1 and ROI_2 , c) ROI_3 and ROI_4 and d) ROI_5

$F_1 = \mu_{Back}$	$F_8 = \mu_{ROI_2}$	$F_{15} = \sigma_{ROI_4}^2$
$F_2 = \sigma_{Back}^2$	$F_9 = \sigma_{ROI_5}^2$	$F_{16} = r_4$
$F_3 = \frac{\sum_{BrT}}{N(BrT)}$	$F_{10} = r_2$	$F_{17} = wr_4$
$F_4 = \frac{\mu_{BrT}}{\mu_{\bar{BrT}}}$	$F_{11} = wr_2$	$F_{18} = \mu_{ROI_5}$
$F_5 = FE(HuT)$	$F_{12} = \mu_{ROI_3}$	$F_{19} = \sigma_{ROI_5}^2$
$F_6 = \mu_{ROI_1}$	$F_{13} = \sigma_{ROI_3}^2$	$F_{20} = r_5$
$F_7 = \sigma_{ROI_1}^2$	$F_{14} = \mu_{ROI_4}$	$F_{21} = wr_5$

Table 1: Features used for breast density estimation.

- T_1 is the threshold derived from MCE at gray level range $[T + 1, 2^8 - 1]$
- T_2 is the threshold derived from MCE at gray level range $[T_1 + 1, 2^8 - 1]$

The value of the threshold T_2 is used to segment the main core of the glandular tissue from the remaining breast area, as figure 2b shows. The lower threshold T_1 results to a larger, more detailed description of the glandular tissue, as observed at figure 2c. Note that all the possible regions combining the two thresholds T_1 and T_2 are extracted, as figure 2 shows. This is due to the importance of the remaining fatty tissue after each segmentation (corresponding to the two thresholds), with regard to shape and size information of the glandular tissue compared to the remaining breast area. So we extract the following regions:

- ROI_1 : the pixels $I(x,y)$ with $0 \leq I(x,y) \leq T_2$.
- ROI_2 : the pixels $I(x,y)$ with $T_2 < I(x,y) \leq 2^8 - 1$.
- ROI_3 : the pixels $I(x,y)$ with $0 \leq I(x,y) \leq T_1$.
- ROI_4 : the pixels $I(x,y)$ with $T_1 < I(x,y) \leq 2^8 - 1$.
- ROI_5 : the pixels $I(x,y)$ with $T_1 < I(x,y) \leq T_2$.

Finally, for each one of the above regions ROI_i , the mean μ_{ROI_i} and the variance $\sigma_{ROI_i}^2$ of the intensities of the pixels are estimated, according to equations (1) and (2) and for the regions ROI_2 , ROI_4 and ROI_5 the features are estimated using equations (7)-(8):

$$r_i = \frac{N(ROI_i)}{N(BrT)} \quad (7)$$

$$wr_i = \frac{\sum_{(x,y) \in ROI_i} I(x,y)}{\sum_{(x,y) \in BrT} I(x,y)} \quad (8)$$

This results to a total number of 21 features, as table 1 shows.

$F_1 = F_{10}^{BRD}$	$F_{14} = \mu_{ROI_2}^{Y-AXIS}$	$F_{27} = ku_{ROI_4}^{Y-AXIS}$
$F_2 = F_{11}^{BRD}$	$F_{15} = \sigma_{ROI_5}^{Y-AXIS}$	$F_{28} = m_{ROI_4}^{Y-AXIS}$
$F_3 = F_{16}^{BRD}$	$F_{16} = sk_{ROI_2}^{Y-AXIS}$	$F_{29} = \mu_{ROI_5}^{X-AXIS}$
$F_4 = F_{17}^{BRD}$	$F_{17} = ku_{ROI_2}^{Y-AXIS}$	$F_{30} = \sigma_{ROI_5}^{X-AXIS}$
$F_5 = F_{20}^{BRD}$	$F_{18} = m_{ROI_2}^{Y-AXIS}$	$F_{31} = sk_{ROI_5}^{X-AXIS}$
$F_6 = F_{21}^{BRD}$	$F_{19} = \mu_{ROI_4}^{X-AXIS}$	$F_{32} = ku_{ROI_5}^{X-AXIS}$
$F_7 = F_5^{BRD}$	$F_{20} = \sigma_{ROI_4}^{X-AXIS}$	$F_{33} = m_{ROI_5}^{X-AXIS}$
$F_8 = N(BrT)$	$F_{21} = sk_{ROI_4}^{X-AXIS}$	$F_{34} = \mu_{ROI_5}^{Y-AXIS}$
$F_9 = \mu_{ROI_2}^{X-AXIS}$	$F_{22} = ku_{ROI_4}^{X-AXIS}$	$F_{35} = \sigma_{ROI_5}^{Y-AXIS}$
$F_{10} = \sigma_{ROI_2}^{X-AXIS}$	$F_{23} = m_{ROI_4}^{X-AXIS}$	$F_{36} = sk_{ROI_5}^{Y-AXIS}$
$F_{11} = sk_{ROI_2}^{X-AXIS}$	$F_{24} = \mu_{ROI_4}^{Y-AXIS}$	$F_{37} = ku_{ROI_5}^{Y-AXIS}$
$F_{12} = ku_{ROI_2}^{X-AXIS}$	$F_{25} = \sigma_{ROI_4}^{Y-AXIS}$	$F_{38} = m_{ROI_5}^{Y-AXIS}$
$F_{13} = \mu_{ROI_2}^{X-AXIS}$	$F_{26} = sk_{ROI_4}^{Y-AXIS}$	

Table 2: Features used for asymmetry detection

3.1.3 Classification

For the classification of the images according to the breast density, Classification and Regression Trees (CARTs) [3] are used. The main motivation for this selection was the simplicity of these trees, as they make no assumption regarding the underlying distributions of the values of the predicted variables. They use simple linear thresholds, resulting to intuitive separation of classes, while there is no need for a feature reduction preprocessing, as CARTs select the informative features themselves. We use three CARTs, equal to the number of the classes. The CART tree Tr_i is trained to output the value 1 for the images of class i and the value 0 for all the remaining images. So we use an unknown pattern as input to all the CART trees and classify to class j , so that $output(Tr_j) = \max_{1 \leq k \leq 3} \{output(Tr_k)\}$, according to the one-against-all classification scheme [17].

3.2 Asymmetry Detection

3.2.1 Feature Extraction

The basic idea in the feature extraction phase is to use the inner segmentation of the breast, already obtained from the mammographic breast density estimation steps, to detect possible asymmetries between a pair of mammograms. For each mammogram, the features described in table 2 are calculated. Note that:

- For each one of the regions ROI_2 , ROI_4 , ROI_5 , consider the pixels in ROI_i as 'on' pixels. In order to find the x-axis cumulative projection in the form of a histogram, estimate the number (sum) of 'on' pixels in every row of the image. In the same way we obtain the y-axis histogram (cumulative projection), as shown in figure 3. Subsequently, estimate the first-order statistics for each of these histograms, meaning mean value μ , standard deviation σ , skewness sk , kurtosis ku and median m .
- The value F_i^{BRD} corresponds to the feature i of the mammographic breast density estimation step (table 1).

The feature vector of length $N = 38$, described in table 2, is estimated for each mammogram. However, in our case, we are interested in detecting asymmetries between a pair of mammograms. Thus, we should detect the cases where the

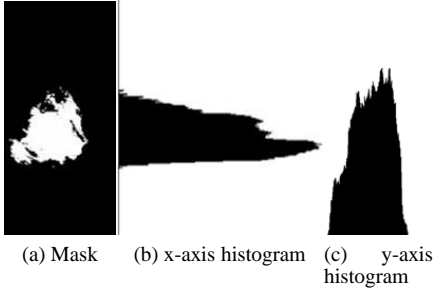


Figure 3: a) Initial Mask, b) x-axis and c) y-axis histogram

values corresponding to the left and the right mammograms differ significantly. Suppose that for the left breast mammogram we have estimated the feature vector f and for the corresponding right breast mammogram the feature vector g . Then, construct the following differential features of equations (9)-(11) that can be used to detect possible asymmetry between a pair of mammographic images:

$$F_{1-38}^{ASYMMD} = \frac{|f_i - g_i|}{\max(f_i, g_i)} \quad (9)$$

$$F_{39-76}^{ASYMMD} = |f_i - g_i| \quad (10)$$

$$F_{77-114}^{ASYMMD} = |f_i - g_i|^3 \quad (11)$$

where $1 \leq i \leq 38$, resulting to a feature space of 114 features in total.

3.2.2 Classification

For the classification of a pair of mammograms according to a possible asymmetry, a modified version of the typical k-nearest neighbor classifier is used. The classifier implemented is described below. Consider a two class problem with classes C_1 and C_2 , containing N_1 and N_2 samples respectively. For an unknown input pattern, w , estimate the k nearest neighbors n_i , $1 \leq i \leq k$, according to Euclidean Distance and then calculate the values of the following variables:

$$sum_1(w) = \frac{N_2}{N_1} \cdot \sum_{\substack{i=1 \\ n_i \in C_1}}^k \frac{1}{d_i} \quad (12)$$

$$sum_2(w) = \frac{N_1}{N_2} \cdot \sum_{\substack{i=1 \\ n_i \in C_2}}^k \frac{1}{d_i} \quad (13)$$

where d_i is the Euclidean Distance of the unknown pattern w to the n_i nearest neighbor.

Then the unknown pattern is classified as:

$$w \in \begin{cases} C_1 & ,if \ sum_1(w) > sum_2(w) \\ C_2 & ,if \ sum_1(w) < sum_2(w) \end{cases} \quad (14)$$

The previous classifier is similar to the a standard k-nn classifier. The difference lies in that the confidence value of each class is multiplied with a constant term, in order to cope with the class imbalance problem [17]. If, for example, class C_1 is oversampled, the constant $\frac{N_2}{N_1}$ (< 1) is multiplied with sum_1 , resulting to a different weight of the patterns of each class.

BREAST DENSITY	TRUE CLASS			
	F	G	D	
PREDICTED CLASS	F	88 (88)	21 (12)	7 (3)
	G	10 (12)	52 (59)	28 (37)
	D	8 (6)	31 (33)	77 (72)

Table 3: Results of the proposed breast density estimation algorithm. Values inside parentheses are the results obtained when using the manual segmentation method.

4. EXPERIMENTS AND RESULTS

The method for evaluating the algorithms is the leave-one-out, which is one of the most common cross-validation methods [17].

4.1 Breast Density Estimation

The proposed mammographic breast density estimation algorithm was tested on all the images of the miniMIAS database, fully annotated according to 3 breast density classes. Note that masks capable of extracting the background, obtained by manual segmentation of the tissue-related areas [19] have been used. Thus, it was possible to compare the results derived by the fully automated and the manually segmented techniques, as it is presented in table 3. Values inside parentheses were the corresponding values, using the manual segmentation. For the evaluation of the algorithm the work in [11] was used, where the Closest Point Distance algorithm proposed achieved 66.15% success rate, while a previous work [1] reported 65%, when applied to a subset of the miniMIAS database. The results of our method achieved a success rate of 67.32%, using the fully automatic segmentation method. As expected, when using the manual segmentation the results were better (68.01%) since the feature extraction procedure used slightly better segmentation data of the mammographic breast area.

4.2 Asymmetry Detection

The proposed asymmetry detection algorithm was applied to all the images of the database, fully annotated as symmetric (SYMM) or asymmetric (ASYMM). The features were processed through univariate significance analysis, specifically T-test [5], resulting to a feature vector of predefined length 18. The results of the algorithm are shown in table 4. Similarly to breast density estimation algorithm, the results derived by the fully automated and the manual segmentation techniques are presented. Values in parentheses are the corresponding results when using the manual segmentation technique. For the evaluation of the algorithm the work presented at [6] was used, where an asymmetry detection technique using Gabor wavelets was presented and tested on 80 images of the miniMIAS database, achieving an average classification accuracy of 74.4%. The results obtained were for the manual segmentation 73.91% and for the automatic method 70.19%. However, note that our method is computationally simpler and more importantly it is based on quantities used in 4.1. Thus our method addresses the tasks of mammographic breast density estimation and asymmetry detection in an unifying context.

BREAST PAIR		TRUE CLASS	
		SYMM	ASYMM
PREDICTED CLASS	SYMM	208 (218)	12 (10)
	ASYMM	84 (74)	18 (20)

Table 4: Results of the proposed asymmetry detection algorithm. Values inside parentheses are the results obtained when using the manual segmentation method.

5. DISCUSSION AND CONCLUSION

The results of this new method for mammographic breast density estimation and asymmetry detection were analyzed and evaluated against all the images of the miniMIAS database. The high level of noise of the images, due to the digitization process, has made the segmentation process an even harder classification task; however the success rate remains high when using the manual ground truth segmentation technique and close to the results produced when using the fully automated segmentation technique [18].

The proposed algorithm for *mammographic breast density estimation* achieves better results than the work at [11] and similar results as the work at [14], which uses only a small portion of the miniMIAS. The work at [2] achieves higher values of success, but it uses textural features, which are computationally very expensive. The work we propose uses simple first order statistics features and a new technique for the power spectrum estimation, making it suitable for real-time applications.

The *asymmetry detection* scheme uses the segmentation already obtained via the breast density estimation procedure. It achieves a success rate similar of the bibliography, although it uses all the images of the miniMIAS database, instead of a small subset, as in [6]. Therefore our experimental results are considered more reliable. Furthermore, the use of the modified version of the k-nn algorithm has been proved a simple yet effective way to overcome the problem of the imbalanced classes.

REFERENCES

- [1] L. Blot and R. Zwigelaar. Background texture extraction for the classification of mammographic parenchymal patterns. In *Medical Image Understanding and Analysis*, pages 145–148, 2001.
- [2] A. Bosch, X. Munoz, A. Oliver, and J. Martí. Modeling and Classifying Breast Tissue Density in Mammograms. In *Proceedings of the 2006 IEEE Computer Society Conference on Computer Vision and Pattern Recognition-Volume 2*, pages 1552–1558. IEEE Computer Society Washington, DC, USA, 2006.
- [3] L. Breiman. *Classification and Regression Trees*. Chapman & Hall/CRC, 1998.
- [4] A. D. Brink and N. E. Pendock. Minimum cross-entropy threshold selection. *Pattern Recognition*, 29(1):179–188, 1996.
- [5] W.W. Cooley and P.R. Lohnes. *Multivariate Data Analysis*. John Wiley & Sons Inc, 1971.
- [6] RJ Ferrari, RM Rangayyan, JEL Desautels, and AF Frere. Analysis of asymmetry in mammograms via directional filtering with Gabor wavelets. *Medical Imaging, IEEE Transactions on*, 20(9):953–964, 2001.
- [7] R.C. Gonzalez and R.E. Woods. *Digital Image Processing*. Prentice Hall, 2007.
- [8] M.J. Homer. *Mammographic Interpretation: A Practical Approach*. McGraw-Hill Companies, 1991.
- [9] LM Kaplan. Extended fractal analysis for texture classification and segmentation. *Image Processing, IEEE Transactions on*, 8(11):1572–1585, 1999.
- [10] S.M. Kwok, R. Chandrasekhar, Y. Attikiouzel, and MT Rickard. Automatic pectoral muscle segmentation on mediolateral oblique view mammograms. *Medical Imaging, IEEE Transactions on*, 23(9):1129–1140, 2004.
- [11] M. Masek, Electronic University of Western Australia School of Electrical, Computer Engineering, and University of Western Australia Centre for Intelligent Information Processing Systems. *Hierarchical Segmentation of Mammograms Based on Pixel Intensity*. PhD thesis, 2004.
- [12] M. Mavroforakis, H. Georgiou, N. Dimitropoulos, D. Cavouras, and S. Theodoridis. Significance analysis of qualitative mammographic features, using linear classifiers, neural networks and support vector machines. *European Journal of Radiology*, 54(1):80–89, 2005.
- [13] R.M. Nishikawa. Current status and future directions of computer-aided diagnosis in mammography. *Computerized Medical Imaging and Graphics*, 31(4-5):224–235, 2007.
- [14] A. Oliver, J. Freixenet, A. Bosch, D. Raba, and R. Zwigelaar. Automatic classification of breast tissue. In *Iberian Conference on Pattern Recognition and Image Analysis*, pages 431–438. Springer, 2005.
- [15] MKJ Siddiqui, M. Anand, PK Mehrotra, R. Sarangi, and N. Mathur. Biomonitoring of organochlorines in women with benign and malignant breast disease. *Environmental Research*, 98(2):250–257, 2005.
- [16] J. Suckling, J. Parker, D. Dance, S. Astley, I. Hutt, C. Boggis, I. Ricketts, E. Stamatakis, N. Cerneaz, S. Kok, et al. The Mammographic Image Analysis Society Digital Mammogram Database. In *Excerpta Medica. International Congress Series*, pages 375–378, 1994.
- [17] S. Theodoridis and K. Koutroumbas. *Pattern Recognition*. Academic Press, 4th edition, 2009.
- [18] St. Tzikopoulos, H. Georgiou, M. Mavroforakis, N. Dimitropoulos, and S. Theodoridis. A fully automated complete segmentation scheme for mammograms. In *16th International Conference on Digital Signal Processing, Santorini, Greece*, July 2009.
- [19] M.A. Wirth. *MIAS Mask Database*. University of Guelph, Canada, 2005.
- [20] JN Wolfe. Risk for breast cancer development determined by mammographic parenchymal pattern. *Cancer*, 37(5):2486–92, 1976.
- [21] F.F. Yin, M.L. Giger, K. Doi, C.J. Vyborny, and R.A. Schmidt. Computerized detection of masses in digital mammograms: Automated alignment of breast images and its effect on bilateral-subtraction technique. *Medical Physics*, 21:445–452, 1994.